

# Anticancer Peptidylarginine Deiminase (PAD) Inhibitors Regulate the Autophagy Flux and the Mammalian Target of Rapamycin Complex 1 Activity<sup>\*[5]</sup>

Received for publication, April 25, 2012, and in revised form, May 15, 2012. Published, JBC Papers in Press, May 17, 2012, DOI 10.1074/jbc.M112.375725

Yuji Wang<sup>†§1</sup>, Pingxin Li<sup>‡1</sup>, Shu Wang<sup>‡1</sup>, Jing Hu<sup>‡</sup>, Xiangyun Amy Chen<sup>‡</sup>, Jianhui Wu<sup>‡§1</sup>, Megan Fisher<sup>‡</sup>, Kira Oshaben<sup>‡</sup>, Na Zhao<sup>‡</sup>, Ying Gu<sup>‡</sup>, Dong Wang<sup>||</sup>, Gong Chen<sup>§2</sup>, and Yanming Wang<sup>‡3</sup>

From the <sup>‡</sup>Center for Eukaryotic Gene Regulation, Department of Biochemistry and Molecular Biology and <sup>§</sup>Department of Chemistry, Pennsylvania State University, University Park, Pennsylvania 16802, the <sup>||</sup>College of Pharmaceutical Sciences, Capital Medical University, Beijing 100069, China, and the <sup>1</sup>Department of Statistics, University of Nebraska, Lincoln, Nebraska 68583

**Background:** Histone citrullination by PAD4 regulates tumor suppressor gene expression.

**Results:** The novel PAD inhibitor YW3-56 inhibits cancerous growth by perturbing autophagy and regulating the SESN2-mTORC1 signaling axis.

**Conclusion:** YW3-56 regulates the SESN2-mTORC1 autophagy pathway as one of its anticancer mechanisms.

**Significance:** This study identifies a novel function of PAD4 in the autophagy pathway and developed potent PAD inhibitors for future cancer research.

Tumor suppressor genes are frequently silenced in cancer cells by enzymes catalyzing epigenetic histone modifications. The peptidylarginine deiminase family member PAD4 (also called PADI4) is markedly overexpressed in a majority of human cancers, suggesting that PAD4 is a putative target for cancer treatment. Here, we have generated novel PAD inhibitors with low micromolar IC<sub>50</sub> in PAD activity and cancer cell growth inhibition. The lead compound YW3-56 alters the expression of genes controlling the cell cycle and cell death, including *SESN2* that encodes an upstream inhibitor of the mammalian target of rapamycin complex 1 (mTORC1) signaling pathway. Guided by the gene expression profile analyses with YW3-56, we found that PAD4 functions as a corepressor of p53 to regulate *SESN2* expression by histone citrullination in cancer cells. Consistent with the mTORC1 inhibition by *SESN2*, the phosphorylation of its substrates including p70S6 kinase (p70S6K) and 4E-BP1 was decreased. Furthermore, macroautophagy is perturbed after YW3-56 treatment in cancer cells. In a mouse xenograft model, YW3-56 demonstrates cancer growth inhibition activity with little if any detectable adverse effect to vital organs, whereas a combination of PAD4 and histone deacetylase inhibitors further decreases tumor growth. Taken together, our work found that PAD4 regulates the mTORC1 signaling pathway and that PAD inhibitors are potential anticancer reagents that activate tumor suppressor gene expression alone or in combination with histone deacetylase inhibitors.

In eukaryotic cells, covalent histone modifications play important roles in regulating gene expression during normal development and in disease etiology (1, 2). Notably, aberrant silencing of tumor suppressor genes by epigenetic modifiers has been recognized as an early onset event during tumorigenesis (3–5). Within the last several decades, small molecule inhibitors against DNA methyltransferases and histone deacetylases have been developed as effective reagents to activate tumor suppressor gene expression in cancer chemotherapy (6). Compounds against novel epigenetic targets, such as Dot1L and Brd4, have been recently reported to effectively inhibit cancerous growth in mouse models (7–9). As such, a new battlefield for cancer treatment is emerging from studies of the epigenetic mechanisms underlying tumorigenesis, which bears promise for the identification of new drug targets and the development of additional pharmacological reagents.

Peptidylarginine deiminases (PADs)<sup>4</sup> are a family of enzymes that can convert protein Arg residues to citrulline in a calcium- and sulfhydryl group-dependent manner. The PAD protein family in human and mouse contains five members, including PAD1–4 and PAD6, that show tissue and substrate specificity (10, 11). PAD1 is mainly expressed in the epidermal keratinocytes (57). PAD6 (also called ePAD) is a protein uniquely expressed in eggs and regulates the early stage of embryonic development, but it misses a conserved cysteine residue at the active center of all other PAD enzymes (12, 13). PAD2 is widely expressed in many tissues, including muscle, brain, and mammary gland, and is found to citrullinate myelin basic protein and actin (10, 11, 14). PAD4 is the only PAD family member containing a nuclear localization signal and citrullinates many sub-

<sup>\*</sup> This work was supported, in whole or in part, by National Institutes of Health Grant R01 CA136856 (to Y. M. W.) from the NCI. This work was also supported by a start-up fund from Pennsylvania State University (to G. C.). In addition, the work was made possible by a PSU Clinical and Translation Science Institute Pilot Grant Award (to G. C. and Y. M. W.).

[5] This article contains supplemental Materials and Methods, Tables S1 and S2, Figs. S1–S9, and Videos S1–S3.

<sup>1</sup> These authors contributed equally to this work.

<sup>2</sup> To whom correspondence may be addressed. E-mail: guc11@psu.edu.

<sup>3</sup> To whom correspondence may be addressed. E-mail: yuw12@psu.edu.

<sup>4</sup> The abbreviations used are: PAD, peptidylarginine deiminase; mTOR, mammalian target of rapamycin; HDAC, histone deacetylase; Cl-amidine, *N*- $\alpha$ -benzoyl-*N*<sup>5</sup>-(2-chloro-1-iminoethyl)-l-ornithine amide; CREB, cAMP-response element-binding protein; MTT, 3-(4,5-dimethylthiazol-2-yl)-2,5-diphenyltetrazolium bromide; RT-qPCR, reverse transcription-quantitative PCR; PUMA, p53 up-regulated modulator of apoptosis; p70S6K, p70S6 kinase; SAHA, suberoylanilide hydroxamic acid; LC3, light chain 3.

strates including histones (e.g. H3, H2A, and H4), p300/CREB-binding protein (CBP), nucleophosmin, ING4, and nuclear lamin C to exert various functions (15–19). Genome-wide association and pathology studies have implicated PAD4 in the etiology of rheumatoid arthritis and cancers in human patients (20–23). We previously found that PAD4 functions as a corepressor of p53 and cooperates with a histone deacetylase HDAC2 to repress the expression of tumor suppressor genes (e.g. p21/*CDKN1A* and *GADD45*) (24, 25). Moreover, PAD4 was recently reported to cooperate with Elk-1 to facilitate *c-fos* expression. As such, PAD4 can positively and negatively regulate transcription in a promoter context-dependent manner (14, 24).

The tumor suppressor p53 protein functions as a central hub and key transcription factor of many cellular signaling pathways (26). In response to DNA damage, starvation, and stress signals, p53 regulates the expression of many genes that in turn relay the upstream signal to determine whether a cell undergoes cell cycle arrest, apoptosis, autophagy, etc. (27–30). Genome-wide mapping efforts have identified several hundred potential p53 target genes (31); many of these p53 target genes are effector proteins or proteins that regulate p53 functions in various positive and negative feedback loops (32). Sestrin 2 (*SESN2*) is a recently identified p53 target gene that regulates aging and induces autophagy by inhibiting the mTORC1 signaling pathway via the AMP-activated protein kinase (AMPK) and TSC1/2 signal cascade (33, 34). Interestingly, *PAD4* was also recently identified as a p53 target gene, suggesting that PAD4 is a component of the intricate p53 signaling network (19, 35), suggesting that PAD4 likely regulates p53 function via a negative feedback loop.

Macroautophagy (hereafter referred as autophagy) is a catabolic cellular process wherein a large number of cytoplasmic components and organelles are engulfed by a membrane structure termed the phagophore to form autophagosomes, which in turn fuse with lysosomes to form autophagolysosomes for bulk degradation to remove damaged cellular organelles or regenerate metabolites during the cellular response to starvation (36–38). Autophagy is an important cellular process for organism health, and its deregulation has been linked with the progression of many human diseases, including neurodegenerative disorders and cancers (36, 39). Many autophagy regulatory factors are evolutionarily conserved from yeast to human, including the mammalian target of rapamycin (mTOR) Ser/Thr kinase-containing mTORC1 protein complex, which senses growth factors and nutrient abundance to control the rate of protein synthesis and the flux of autophagy (38, 40). The Yin-Yang balance of autophagy flux is key to maintaining the homeostasis between cell survival and cell death. The metabolites recycled through autophagy can sustain cell survival and contribute to chemotherapy resistance (41). On the other hand, under circumstances of excessive degradation of cellular components, autophagy can result in cell death (42). Therefore, both inducers and inhibitors of autophagy are of potential value for cancer treatment by regulating the autophagy flux rate.

Under physiological conditions, PAD4 is mainly expressed in peripheral blood neutrophils. We have previously found that PAD4 plays an antibacterial innate immune function through

regulating the formation of neutrophil extracellular traps (43). On the other hand, PAD4 is markedly overexpressed in a majority of cancers of various tissue origins in pathology studies with a large cohort of human patient samples (21), suggesting that PAD4 may play a role in tumorigenesis. Currently, it remains unknown whether PAD4 can be pharmacologically targeted for cancer treatment. Cl-amidine is a benzoyl-arginine-derived and mechanism-based pan PAD inhibitor that shows inhibitory effects to several PAD family members (44, 45). However, this compound causes cancer cell growth inhibition at ~150–200  $\mu\text{M}$  concentration in cultured cells (24, 25). The relatively low potency of Cl-amidine limits its preclinical exploration in cancer study and treatment. We have tested the idea that efficient small molecule PAD inhibitors can epigenetically activate tumor suppressor genes, thereby offering new avenues for cancer research and treatment. Our results showed that the lead compound YW3-56 activates a cohort of p53 target genes, including *SESN2*, which in turn inhibits the mTORC1 signaling pathway, thereby perturbing autophagy and inhibiting cancerous cell growth.

## EXPERIMENTAL PROCEDURES

**Chemical Synthesis and Colorimetric Assays of PAD4 Inhibitors**—The method for chemical synthesis of novel PAD4 inhibitors was done largely following a method described previously (44). The colorimetric PAD4 assay method is described in detail in the [supplemental material](#).

**Cell Culture and Treatment with Compounds and siRNA**—Human osteosarcoma U2OS and mouse sarcoma S-180 cells were purchased from ATCC and cultured in Dulbecco's modified Eagle's medium (DMEM) supplemented with 10% fetal bovine serum and 1% penicillin-streptomycin in a 5%  $\text{CO}_2$  incubator. Early passage cells were used to minimize passage deviations. U2OS p53-shRNA and U2OS Ctrl-shRNA cells were generated essentially as described previously (25). Concentrations and duration of YW3-56 treatment were performed as specified in the figure legends and text of the current study. For the starvation assay, U2OS cells were first cultured in serum-free DMEM for 16 h and then in 10% fetal bovine serum, then different concentrations of YW3-56 were added back, and cells were further incubated for 8 h before additional analyses. *SESN2* siRNA (Santa Cruz Biotechnology) and GFP siRNA (Dharmacon Inc.) were transfected into U2OS cells using the X-tremeGENE siRNA transfection reagents (Roche Applied Science). Cells were incubated in the presence of the siRNA for 48 h before adding YW3-56 and further incubated for 8 h before analyses.

**MTT and Flow Cytometry Assays**—Details of MTT and flow cytometry assays can be found in the [supplemental material](#).

**Transmission Electron Microscopy and Phase Contrast Microscopy**—U2OS Cells were treated with 6  $\mu\text{M}$  YW3-56 for 24 h and fixed in 2% glutaraldehyde in 0.1 M phosphate buffer, pH 7.4. Transmission electron microscopy analyses of U2OS cell morphology were performed using the service of the Penn State Electron Microscopy Facility. A VistaVision invert microscope (VWR International, LLC) equipped with a SPOT Insight digital camera (Diagnostic Instruments, Inc.) and a 10 $\times$  phase

contrast lens were used to analyze cell growth and morphology in phase contrast microscopy analyses.

**RNA Extraction, Microarray, Reverse Transcription, and Quantitative PCR**—Details of these methods can be found in the supplemental material.

**Western Blot and Fluorescent Imaging**—Western blot and immunostaining were performed essentially as described previously (25). Antibodies used in Western blot were anti-p53 (Sigma, BP53-12), anti-PAD4 (custom-made), anti-H3Cit (Abcam, ab5103), anti-H3 (Abcam, ab1791), anti-p21 (Sigma, P1484), anti-PUMA (Calbiochem, PC686), anti-SESN2 (Abcam, ab57810), anti-p70S6K (Cell Signaling, 9202), anti-p70S6K-pT389 (Cell Signaling, 9205), anti-LC3B (Cell Signaling, 2775), anti-p62/SQSTM1 (Bethyl Laboratories, A302-855A), and anti- $\beta$ -actin (Sigma, A1978) at the appropriate dilutions. Anti-LC3B antibody (Cell Signaling, 2775) was used for immunostaining. DNA was stained by the DNA dye Hoechst. For subcellular localization of YW3-56, U2OS cells were treated with YW3-56 for 12 h and then fixed in 3.7% paraformaldehyde in PBS buffer containing 0.1% Triton X-100 and 0.2% Nonidet P-40, pH 7.4. Nuclear DNA was visualized by TOPRO3 staining and captured using an Olympus BX61 microscope at excitation 647 nm/emission 665 nm. Images of YW3-56 subcellular distribution were captured at excitation 359 nm/emission 461 nm.

**Chromatin Immunoprecipitation (ChIP) Assay**—ChIP experiments were carried out essentially as described previously (14). Antibodies used in ChIP were: anti-p53 (Sigma, BP53-12), anti-PAD4 (custom-made), anti-H3Cit (Abcam, ab5103), and anti-H3R17Me (Abcam, ab8284). Primers used in quantitative ChIP-qPCR for +733 are listed in supplemental Table S2. Other primers are available upon request.

**In Vivo Antitumor Assay**—S-180 ascites tumor cells were used to form solid tumors after subcutaneous injection essentially as described previously (46). More details are available in the supplemental material. All animal experiments were approved by the Institutional Animal Care and Use Committee of Capital Medical University and performed by accepted veterinary standards.

## RESULTS

**Novel PAD Inhibitors with Increased Ability to Inhibit PAD4 and Cancer Cell Growth**—To develop more potent inhibitors for PAD4 inhibition and cancer cell killing, we carried out an extensive structure-and-activity relationship study based on the Cl-amidine blueprint (Fig. 1A). The  $N\alpha$  and  $C\alpha$  of the ornithine backbone were engineered with different structural motifs or tethered within a ring scaffold via the standard amide- and ester-coupling chemistry to generate 23 new compounds in four synthesis, evaluation, and redesign cycles (supplemental Fig. S1). Cl-amidine is a very hydroscopic compound, which readily dissolves in water-based solutions and likely has low cell membrane permeation ability. Therefore, one of the design schemes was to optimize the hydrophobicity and bioavailability of the new compounds. The 23 compounds were first used at 20  $\mu$ M to measure their cell-killing efficacy in osteosarcoma U2OS cells by MTT assays (supplemental Fig. S2). Several potent inhibitors (e.g. YW3-56, YW4-03, and YW4-15) were selected

to measure their  $IC_{50}$  in cell killing by MTT assays and PAD4 inhibition by a colorimetric method (47) (supplemental Fig. S3). Inhibitors with low micromolar  $IC_{50}$  values, including YW4-03 and YW3-56, were successfully developed (Fig. 1B).

When compared with Cl-amidine, YW3-56 showed >60-fold increase in cell growth inhibition efficacy ( $IC_{50}$  about 2.5  $\mu$ M) but only ~5-fold increase in PAD4 inhibition ( $IC_{50}$  about 1–5  $\mu$ M) (Fig. 1B). We postulated that the dimethyl-amide-naphthalene moiety at the  $N\alpha$  position and a phenyl ring at the  $C\alpha$  position increase the hydrophobicity of YW3-56, thereby enhancing its membrane permeability and cancer cell killing. To test this idea, flow cytometry analyses were performed to evaluate cellular uptake of YW3-56 using the intrinsic fluorescent signal generated by the naphthalene moiety in YW3-56 (Fig. 1C). Fluorescent signals were greatly increased in all cells after YW3-56 treatment when compared with untreated cells (Fig. 1C). To further test the importance of membrane permeation in cell killing, a bulky and hydrophilic biotin moiety was added on the *para* position of the  $C\alpha$  benzyl ring of YW3-56 to generate YW4-15. This biotin moiety greatly decreased the cellular uptake of YW4-15 in flow cytometry analyses (Fig. 1C). As a consequence of poor membrane penetration, although YW4-15 has a PAD4 inhibition efficacy similar to YW3-56, its cancer cell killing ability was greatly decreased when compared with YW3-56 (Fig. 1B). Taken together, the above results indicate that YW3-56 has an improved efficacy in PAD4 inhibition and cell membrane penetration and thereby kills cancer cells with high efficacy.

Based on the above results, we chose YW3-56 as the lead compound for further detailed biological analyses. Taking advantage of the fluorescent naphthalene moiety, we analyzed the subcellular distribution of YW3-56 and found that it is mainly concentrated in the nucleus, with a certain degree of enrichment in the nucleolus to form punctate structures (Fig. 2A). Because PAD4 is a nuclear protein, the nuclear localization of YW3-56 indicates that it is in the same subcellular compartment as PAD4. The nucleolar localization of YW3-56 is notable given that nucleophosmin, an abundant protein in the nucleolus, is a known substrate of PAD4 (35, 48). Furthermore, we analyzed the dose-dependent effects of YW3-56 on cell morphology and growth. At 2–4  $\mu$ M concentrations, YW3-56 displayed mainly cytostatic effects by slowing cell division, whereas at higher concentrations, it exerted cytotoxic effects by altering cell morphology and killing cells (supplemental Fig. S4). Recently, PAD4 and to a lesser extent PAD2, but not PAD3, were reported to citrullinate histone H3 (11). Given our interest in understanding histone citrullination in gene regulation, we next evaluated the target specificity of YW3-56 to PAD4 and PAD2 using histone H3 as a substrate. Consistent with the previous study (11), PAD2 had a weaker activity toward histone H3 when compared with PAD4 (Fig. 2B). On the other hand, using histone H3 as a substrate, the  $IC_{50}$  of YW3-56 in PAD4 inhibition is about 1–2  $\mu$ M, whereas its  $IC_{50}$  in PAD2 inhibition is about 0.5–1  $\mu$ M (Fig. 2C). Due to its inhibitory activity to PAD2, YW3-56 is referred to as a PAD inhibitor hereafter.

**YW3-56 Induces p53 Target Genes and Regulators of mTORC1**—To analyze the molecular mechanisms by which YW3-56 induces cancer growth inhibition, we performed

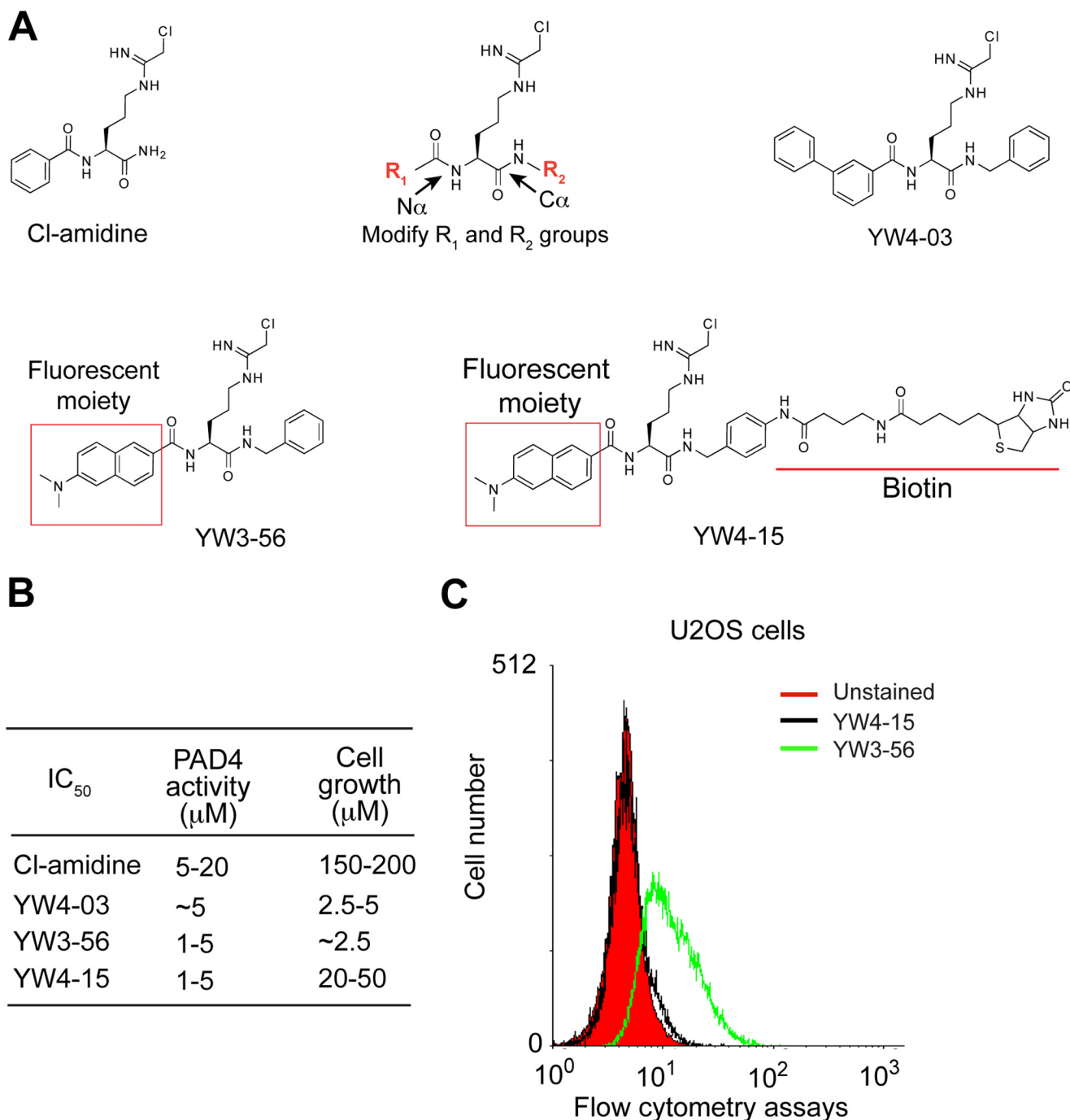


**FIGURE 1. Synthesis and characterization of more potent PAD4 inhibitors.** A, structures of PAD4 inhibitors, including the prototype inhibitor Cl-amidine (upper left panel), the generic structure for medicinal chemistry modification (upper middle panel), the new compound YW4-03 (upper right panel), the lead compound YW3-56, and its biotin-conjugated form YW4-15. YW3-56 and YW4-15 are intrinsically fluorescent molecules because of the dimethyl-amide-naphthalene moiety. B, tabulation of the IC<sub>50</sub> values of cell growth and PAD4 inhibition by several representative inhibitors. IC<sub>50</sub> for PAD4 inhibition was measured using colorimetric assays. IC<sub>50</sub> for cell growth inhibition was measured by MTT assays in the above three independent experiments. C, flow cytometry assays to measure the accumulation of YW3-56 and its biotin-conjugated form YW4-15 after 10 μM of compound treatment for 12 h (a representative result of three repeats is shown).

microarray analyses using Affymetrix microarray chips. Using a 1.5-fold change as the cutoff ( $n = 3$ , false discovery rate  $<0.05$ ), 843 genes were induced, whereas 646 genes were repressed after YW3-56 treatment in U2OS cells. Gene ontology analyses found that the cell cycle, nucleosome assembly, gene regulation, and cell death pathway genes were significantly enriched (Fig. 3A). Within the group of genes of the nucleosome assembly pathway, the expression of multiple histone genes was

decreased by severalfold (supplemental Fig. S5, A and B). The decreased histone gene expression was further analyzed using reverse transcription quantitative PCR (RT-qPCR) to corroborate the microarray results (supplemental Fig. S5C). Both microarray and RT-qPCR assays detected a significant decrease of histone genes, suggesting that YW3-56 can impact on the cell cycle progression by inhibiting histone gene expression via mechanisms yet to be characterized in future research. More-

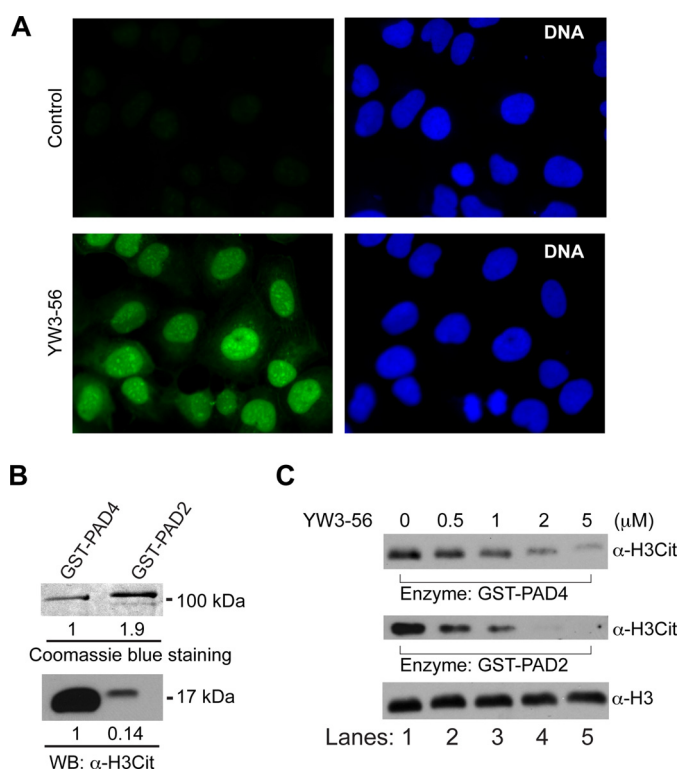


**FIGURE 2. Subcellular localization of YW3-56 and its inhibition of PAD4 and PAD2 activity.** A, upon the addition of YW3-56 to U2OS cells, the subcellular localization of YW3-56 (green color) was visualized by fluorescent microscope. B, comparison of the GST-PAD4 and GST-PAD2 activity using histone H3 substrate in Western blot (WB) experiments. C, different amounts of YW3-56 were preincubated with PAD2 and PAD4. Enzymatic activity toward histone H3 substrate after inhibitor incubation was detected by Western blot experiments. The total amount of H3 was probed with a general histone H3 antibody. Representative results of over three repeats experiments are shown in panels A–C.

over, because PAD4 regulates the expression of p53 target genes (24, 25), we compared our microarray gene list with the 122 direct p53 target genes reported previously (31). 14 genes identified in the microarray analyses overlap with the p53 target genes, representing a significant enrichment of p53 genes (14/122,  $p < 0.01$ ) (Fig. 3A). To show the consistency of the three independent microarray experiments, heat maps of 356 genes showing an average of  $\geq 2$ -fold increase and 227 genes showing an average  $\geq 2$ -fold decrease are presented (Fig. 3B). In contrast to the primary decrease in histone gene expression, genes of the p53 pathway were mainly up-regulated after YW3-56 treatment (supplemental Table S1). Notably, two upstream regulators of the mTOR signaling pathway, *SESN2* and *DDIT4* (also called REDD1), were induced 6.1- and 4.2-fold, respectively, after YW3-56 treatment (supplemental Table S1). Both *SESN2* and *DDIT4* repress the mTORC1 kinase activity through the TSC1/2 signaling axis (33, 49), suggesting that YW3-56 treatment may impact on the *SESN2/DDIT4*  $\rightarrow$  TSC1/TSC2  $\rightarrow$  mTORC1 signaling axis.

To assess the importance of p53 in YW3-56-mediated cell growth inhibition, we performed MTT assays in U2OS cells with or without p53 depletion by shRNA. Depletion of p53 constantly attenuated the cell growth inhibition efficacy of YW3-56 (supplemental Fig. S6A, \* indicates  $p < 0.02$ ), suggesting that the relative abundance of p53 plays a role in YW3-56-induced

cell killing in U2OS cells. RT-qPCR analyses showed a decrease in p53 mRNA after the p53 shRNA treatment (Fig. 4A). The basal level of *SESN2*, p21/*CDKN1A*, and *PUMA* expression was decreased by p53 depletion (Fig. 4A and supplemental Fig. S6B). In contrast, the basal level expression of *DRAM* (damage-regulated autophagy modulator), *AMPK*, *PIG3*, and *BAX* was not affected by p53 depletion (Fig. 4A and supplemental Fig. S6B). After YW3-56 treatment, the expression of *SESN2*, p21/*CDKN1A*, and *PUMA* was strongly induced in control shRNA-treated U2OS cells but induced to a relatively lower amount in p53-depleted cells (Fig. 4A and supplemental Fig. S6B). The expression of mTOR regulator *SESN2* but not *AMPK* was increased after YW3-56 treatment in a p53-dependent manner, suggesting that YW3-56 specifically activates a subset of mTOR regulatory genes (Fig. 4A). Moreover, the relatively less potent inhibitors YW3-88 and BL1-07 induced the expression of p53 target genes, including *SESN2*, at higher concentrations, suggesting that multiple PAD inhibitors can exert similar effects on gene activation in U2OS cells (supplemental Fig. S7).

**PAD4 Serves as a Corepressor of p53 to Directly Regulate *SESN2* Expression**—To analyze whether YW3-56 primarily targets PAD4 to exert its effects on histone citrullination and *SESN2* expression, we treated U2OS cells with YW3-56 and PAD4 siRNA. Both YW3-56 treatment and siRNA depletion of PAD4 activated *SESN2* expression and decreased histone H3 citrullination (Fig. 4B), suggesting that PAD4 plays a direct role in regulating *SESN2* expression. Moreover, depletion of PAD4 sensitizes cell responses to YW3-56 treatment, showing a further decrease in histone H3 citrullination and increase in *SESN2* expression (Fig. 4B). Although YW3-56 was found to inhibit PAD2 and PAD4, the histone H3 citrullination activity of PAD2 is much weaker *in vitro* (Fig. 2C), and PAD2 preferentially localizes to the cytoplasm (50). The above results indicate that PAD4 is the main enzyme responsible for histone H3 citrullination and a main target of YW3-56 in regulating the *SESN2* expression. On the other hand, it remains possible that YW3-56 impacts on PAD2 in other aspects of its anticancer activity.

Although *SESN2* was reported as a p53 target gene, the direct evidence for p53 binding on a specific region of the *SESN2* promoter is not available according to our knowledge. To map p53 binding site(s) at the *SESN2* gene, we performed ChIP experiments using a set of primers spanning regions of the *SESN2* gene with putative p53 binding consensus sites predicted by the PROMO program (Fig. 4C). The binding of p53 to the +733 position of *SESN2* was increased  $\sim 8$ -fold after UV irradiation treatment in U2OS cells (Fig. 4D), suggesting that this region contains putative p53 binding sites. Moreover, p53 binding at the +733 position of *SESN2* was increased  $> 4$ -fold with a concomitant increase of histone H3 Arg-17 methylation (H3R17Me) after YW3-56 treatment (Fig. 4E). In contrast, a decrease in PAD4 binding and histone H3 citrullination (H3Cit) at the +733 position was detected after YW3-56 treatment (Fig. 4E). The above results support a model in which PAD4 serves as a corepressor of p53 to repress *SESN2* expression in untreated cells. In contrast, after YW3-56 treatment, p53 associates, whereas PAD4 dissociates from, the *SESN2*

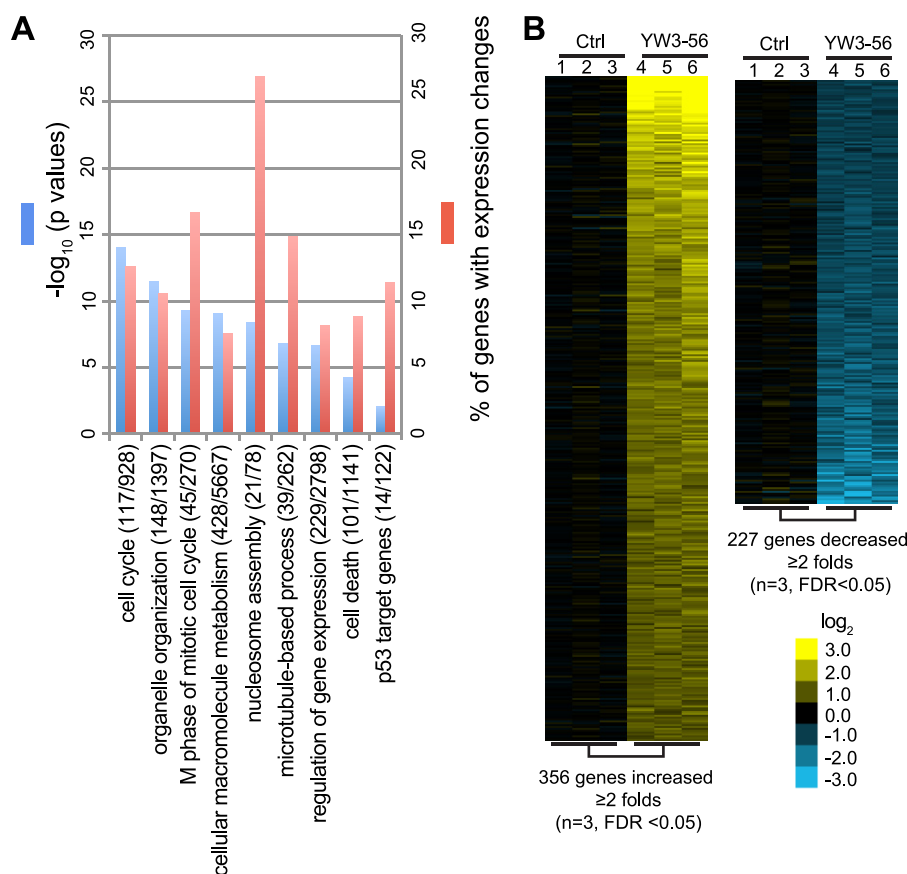


**FIGURE 3. Cellular functions of genes affected by YW3-56 treatment.** A, genes with changed expression after 8  $\mu\text{M}$  YW3-56 treatment for 8 h were analyzed according to their gene ontology categories. Gene ontology terms are shown on the x axis together with the number of genes changed/the number of genes with that category shown in parentheses. The scale for the  $\log_{10}$  p values for the enrichment significance is graphed along the left side of the y axis, and the scale for the percentages of genes showing changes within each category is graphed along the right side of the y axis. B, heat map of genes showing  $\geq 2$ -fold increased expression from three independent experiments (left columns) and genes showing  $\geq 2$ -fold decreased expression from three independent experiments (right columns). Each column represents an independent experiment. Yellow color indicates genes of increased expression, whereas blue color indicates genes of decreased expression after YW3-56 treatment. FDR, false discovery rate. Ctrl, control.

gene, allowing a decrease in H3Cit and an increase in H3R17Me to activate *SESN2* expression.

**Role of *SESN2* in YW3-56-mediated Inhibition of the *mTORC1* Signaling**—*SESN2* is induced by starvation and stress conditions and serves as an upstream inhibitor of *mTORC1* by forming a complex with *TSC1/2* (33). *mTORC1* inhibition decreases its phosphorylation of p70S6K and 4E-BP1, thereby inhibiting translation, cell growth, and proliferation, whereas accelerating autophagy (17, 18) (illustrated in Fig. 5A). Next, we analyzed whether YW3-56 inhibits the *mTORC1* signaling cascade by *SESN2* induction. The amount of *SESN2* protein was increased by YW3-56 in U2OS cells treated with control shRNA (Fig. 5B, lanes 1–4). In contrast, depletion of p53 by shRNA decreased the basal level of *SESN2* and its induced levels after YW3-56 treatment (Fig. 5B, lanes 5–8), indicating that p53 is important for the relative levels of *SESN2* expression. It is noteworthy that *SESN2* expression can be induced at higher YW3-56 concentrations (Fig. 5B, lane 8), suggesting that a low level of p53 in p53-depleted U2OS cells is sufficient for YW3-56-mediated *SESN2* induction. Although the amount of p70S6K protein was not altered in U2OS cells treated with YW3-56 at different concentrations (Fig. 5B, lanes 1–4), the depletion of p53 decreased the amount of p70S6K protein regardless of inhibitor treatment (Fig. 5B, lanes 5–8). In agree-

ment with the inhibitory role of *SESN2* in the *SESN2*-*TSC1/2*-*mTORC1* signaling axis, the induction of *SESN2* by YW3-56 occurred with a concomitant decrease in p70S6K phosphorylation at Thr-389 (Fig. 5B). Furthermore, the inhibitory effects of YW3-56 on histone H3 citrullination were detected in U2OS cells treated with the control or the p53 shRNA (Fig. 5B).

To test whether YW3-56 induces *SESN2* and inhibits *mTOR* under stress conditions, we treated serum-starved U2OS cells with YW3-56 or a combination of YW3-56 and serum. Under serum starvation and serum stimulation conditions, YW3-56 treatment induced *SESN2* expression and dramatically decreased the phosphorylation of p70S6K as well as another *mTORC1* target protein 4E-BP1 (Fig. 5C). The phosphorylation of 4E-BP1 plays an important role in translation by regulating its binding to the translation initiation factor eIF-4E (40, 51). To further assess the role of *SESN2* in YW3-56-mediated *mTORC1* inhibition, we used siRNAs to deplete *SESN2* in U2OS cells. Depletion of *SESN2* slightly increased p70S6K protein levels but drastically increased its phosphorylation levels (Fig. 5D, lane 3 as compared with lane 1), suggesting that *SESN2* is important for regulating p70S6K phosphorylation in cells without YW3-56 treatment. On the other hand, YW3-56 dramatically decreased p70S6K phosphorylation in cells treated with the control GFP siRNA (Fig. 5D, lane 2 as com-

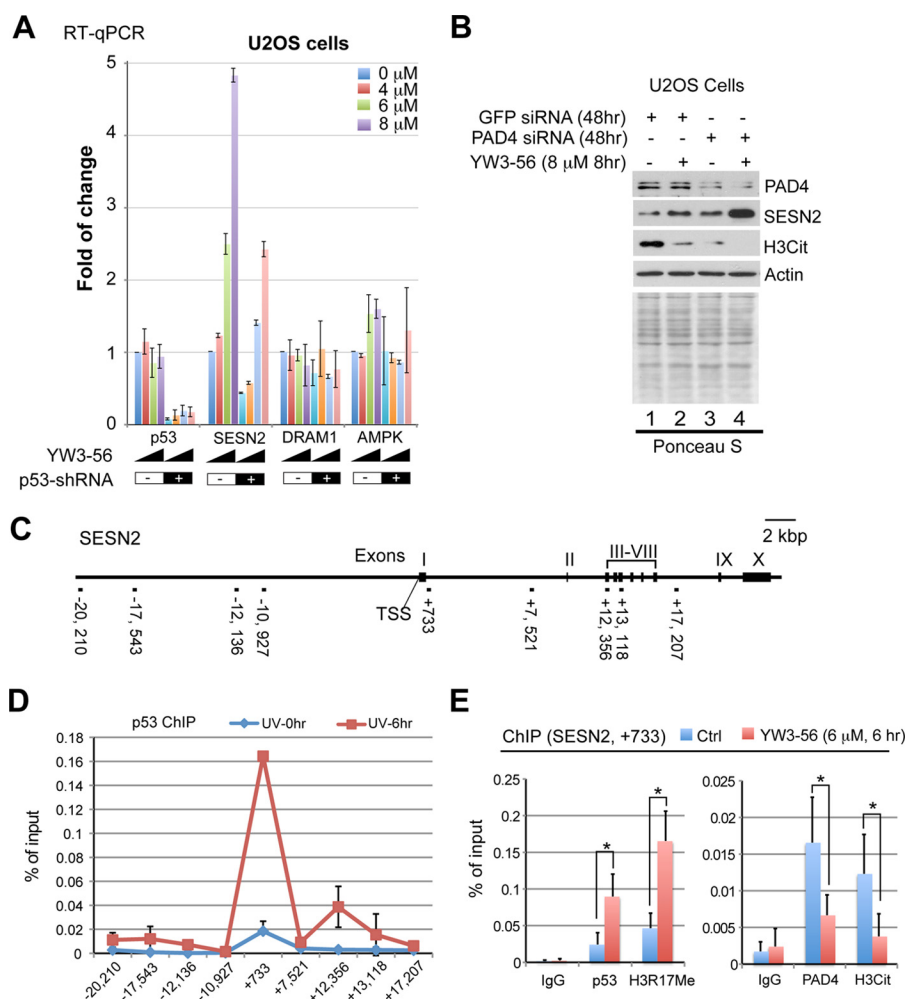


**FIGURE 4. Direct regulation of the *SESN2* expression by p53 and PAD4.** A, RT-qPCR analyses of p53 and its target gene expression after 6 h of YW3-56 treatment of U2OS cells with or without p53 depletion by shRNA. The expression levels of each gene in control U2OS cells without p53 depletion and YW3-56 treatment were normalized to 1. Averages and standard deviations are shown ( $n = 3$ ). B, representative Western blot results of the effects of YW3-56 on histone H3 citrullination and SESN2 expression in U2OS cells with or without PAD4 siRNA treatment. C, schematic illustration of the *SESN2* gene intron and exon structure organization. Coordinates of the primers used to probe for p53 and PAD4 binding are indicated. TSS position is set as +1. D, ChIP analyses of p53 binding at the *SESN2* gene before and after UV irradiation treatment for 6 h. E, ChIP analyses of p53 and PAD4 association as well as histone H3R17Me and H3Cit modifications at the +733 position of *SESN2* gene before and after YW3-56 treatment at 6  $\mu$ M for 6 h. Averages and standard deviations ( $n = 2 \times 3$ ) are shown (\* indicates  $p < 0.005$ ). TSS, transcription start site.

pared with *lane 1*), whereas p70S6K phosphorylation was only slightly decreased after YW3-56 treatment in SESN2 depletion cells (Fig. 5D, *lane 4* as compared with *lane 3*), suggesting that SESN2 is important for YW3-56-mediated inhibition of p70S6K phosphorylation. Taken together, the above results indicate that YW3-56 treatment can induce the expression of SESN2, which in turn triggers a cascade of signaling events to inhibit the mTORC1 kinase activity.

**YW3-56 Regulates the Autophagy Flux**—The induction of upstream inhibitors of the mTORC1 pathway, which keeps the Yin-Yang balance of translation and autophagy, prompted us to analyze whether YW3-56 treatment regulates autophagy in U2OS cells. In transmission electron microscopy (TEM) analyses, many large vesicles containing engulfed and digested membrane and organelle structures were observed in YW3-56-treated cells but not in control cells (Fig. 6A and supplemental Fig. S8). These large vesicular structures (denoted by *red arrows*) have structural characteristics of autophagic vesicles (*e.g.* autophagosomes and autophagolysosomes) (52). The for-

mation of phagophores and autophagosomes is associated with lipidation of LC3-I with phosphatidylethanolamine to produce the membrane-associated LC3-II protein (52). Consistent with autophagic vesicle accumulation, LC3-II accumulated after YW3-56 treatment in a drug dose-dependent manner (Fig. 6B). Furthermore, LC3 staining was detected in multiple large punctate structures in U2OS cells after YW3-56 treatment but not in control cells (Fig. 6C), offering additional evidence for the formation of autophagosomes and/or autophagolysosomes after YW3-56 treatment.

The flux rate of autophagy can be controlled by several steps: 1) the enclosure of cytoplasmic components by phagophores to form autophagosomes; 2) the fusion of autophagosomes with lysosomes to form autophagolysosomes; 3) the dissolution of autophagolysosomes (illustrated in Fig. 6D). To analyze how YW3-56 affects the stepwise progression of autophagy, we performed live cell imaging using an mCherry-GFP-LC3 reporter construct. The GFP signal in the mCherry-GFP-LC3 fusion protein is quenched under acidic pH in autophagolysosomes,

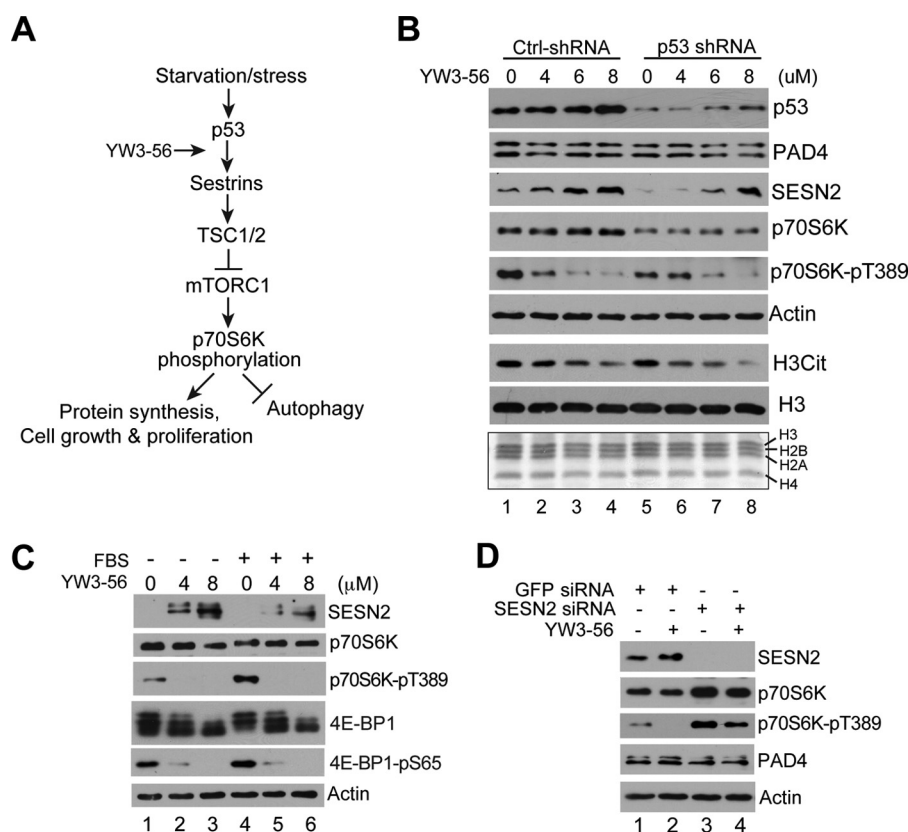


**FIGURE 5. YW3-56 regulates the mTOR signaling pathway through SESN2 induction.** A, illustration of the p53-SESN2-mTORC1 signaling pathway. SESN2 forms complex with TSC1/2 to inhibit the mTORC1 activity and subsequent p70S6K phosphorylation, which offers a molecular mechanism linking YW3-56 treatment to autophagy regulation. B, the levels of p53, PAD4, SESN2, and p70S6K proteins, the phosphorylation of p70S6K at Thr-389, and the citrullination of histone H3 were analyzed by Western blot experiments in U2OS cells treated with different doses of YW3-56 for 8 h. p53 was depleted by shRNA to analyze its effects on cellular response to YW3-56 treatment. Actin was probed to ensure equal protein loading. The amount of histones in each lane was monitored by Ponceau S staining for equal loading. C, Western blot analyses were performed to analyze SESN2, p70S6K, p70S6K Thr-389 phosphorylation, 4E-BP1, and 4E-BP1 Ser-65 phosphorylation after YW3-56 treatment for 8 h in U2OS cells with or without serum starvation. Actin was probed to ensure equal protein loading. D, Western blot analyses were performed to analyze the effects of SESN2 depletion on p70S6K phosphorylation in U2OS cells without or with YW3-56 treatment for 8 h. Representative results of over three repeats experiments are shown in panels B–D. Ctrl, Control.

making it a nice fluorescent sensor to simultaneously analyze autophagosomes and autophagolysosomes (52, 53). We found that ectopically expressed mCherry-GFP-LC3 was detected as predominantly red and dynamically moving spots with yellow spots occasionally observed in control U2OS cells, suggesting that the reporter protein was mainly associated with autophagolysosomes (Fig. 6E and supplemental Video S1). In contrast, after treatment with YW3-56, enlarged red and yellow speckles with reduced movement were observed in cells remaining attached to the culture surface (Fig. 6F and supplemental Video S2) and in moribund cells that were shrinking in size and partially losing their attachment with the culture surface (Fig. 6G and supplemental Video S3), indicating that both autophagosomes and autophagolysosomes were accumulated after YW3-56 treatment. Due to its selective degradation during autophagy, p62 (also called sequestosome 1, SQSTM1) serves as a marker for autophagy, and its cellular level inversely correlates with the rate of autophagic vesicle degradation (52). We found that p62 dramatically accumulated in YW3-56-treated cells in a dose-dependent manner (Fig. 6B), suggesting that YW3-56 regulates the autophagy flux by inhibiting autophagic vesicle breakdown by lysosomes. Two scenarios may lead to the accumulation of autophagic vesicles: first, an increase in the influx rate with more autophagosome feeding

into the autophagy process; and second, a decrease in the efflux rate with the less efficient fusion of autophagosomes with lysosomes and subsequent autophagolysosome dissolution. Note that these two possible mechanisms are not mutually exclusive and can function independently or in combination. Our results suggest that YW3-56 may induce the accumulation of autophagosomes by inhibiting mTORC1 as well as inhibiting autophagosome degradation to slow down the autophagy flux rate.

**YW3-56 Effectively Inhibits Cancer Growth in Mouse Sarcoma S-180 Xenograft Model**—To test the effects of YW3-56 on tumor growth in mice, we applied a well established mouse sarcoma S-180 cell-derived tumor model (54). MTT assays showed that YW3-56 inhibited S-180 cell growth with an  $IC_{50}$  of  $\sim 10$ – $15 \mu M$  (Fig. 7A). RT-qPCR analyses showed that YW3-56 treatment induced the expression of p53 and its target genes, including *SESN2*, in a concentration-dependent manner (Fig. 7B). Upon intraperitoneal injection of YW3-56 at a concentration of 10 mg/kg of mouse body weight daily for 1 week, the growth of S-180 tumor was decreased to  $\sim 51.5\%$  of that of the control group injected with an isotonic saline solution (Fig. 7, C and D). The HDAC inhibitor SAHA (also called vorinostat) is a United States Food and Drug Administration-approved drug for treatment of cutaneous T cell lymphoma. As a reference to evaluate the effect of YW3-56, we injected SAHA at 5

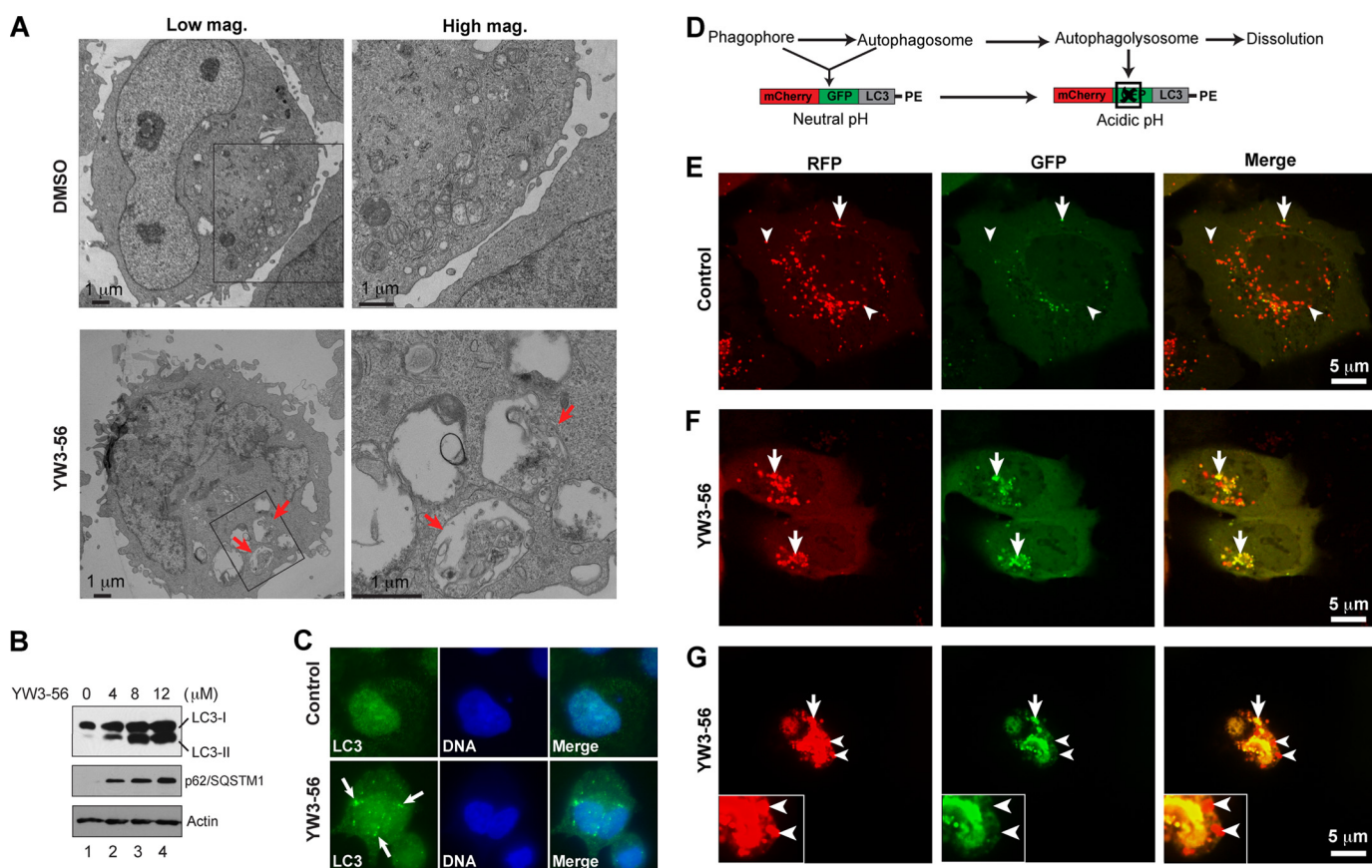


**FIGURE 6. YW3-56 induces autophagy in human osteosarcoma U2OS cells.** *A*, transmission electron microscopy images of mock-treated cells at low magnification (*Low mag.*) and high magnification (*High mag.*) (*upper panels*) as well as YW3-56-treated cells (*lower panels*). Distinctive structures with characteristics of autophagolysosomes in YW3-56-treated cells are denoted by *red arrows*. Scale bars are 1 μm. *B*, levels of LC3-I and LC3-II as well as p62/SQSTM1 were analyzed by Western blot after different doses of YW3-56 treatment for 12 h. *C*, LC3 was detected in large speckles denoted by *white arrows* in U2OS cells after YW3-56 treatment cells (*lower panels*) but not in control cells (*upper panels*). *D*, schematic drawing of the autophagy process. The mCherry-GFP-LC3-PE reporter is *red* and *green* when it associates with phagophores (also called isolation membranes) and autophagosomes (PE denotes phosphatidylethanolamine). After fusion with lysosomes to form autophagolysosomes, the GFP signal is quenched by the acidic condition. *E*, a representative microscopy image showing *red-colored* autophagolysosomes and *red and green double-colored* autophagosomes in control mock-treated cells. See *video S1* for more details. *F*, a representative microscopy image showing *red-colored* autophagolysosomes and *red and green double-colored* autophagosomes in YW3-56-treated cells with slight morphology changes. See *video S2* for more details. *G*, a representative microscopy image showing *red-colored* autophagolysosomes and *red and green double-colored* autophagosomes in a moribund cell after YW3-56 treatment. *Insets* show details of the structures at higher magnification. *Arrowheads* denote autophagolysosomes, and *arrows* denote autophagosomes (*E–G*). Scale bars in panels *E–G* represent 5 μm.

mg/kg of body weight concentration daily for 1 week and found that S-180-derived tumor growth was decreased to ~44.6% of that of the control group (Fig. 7, *C* and *D*). As such, YW3-56 showed a similar tumor growth inhibition effect as that of SAHA under the conditions applied. Additionally, because we have found that PAD4 coordinates with HDAC2 in repressing p53 target gene expression (25), we tested the synergy of the PAD4 inhibitor and HDAC inhibitor in tumor growth. We found that after injection of a mix of YW3-56 and SAHA at half of their concentrations when applied singularly, tumor growth was decreased to ~27.1% of that of the control group (Fig. 7, *C* and *D*), suggesting an additive effect of the two inhibitors. In comparison with doxorubicin, a well established chemotherapeutic reagent, a mixture of YW3-56 and SAHA showed cancer growth inhibition effect close to that of doxorubicin applied at 2 mg/kg of body weight concentration (Fig. 7, *C* and *D*).

To evaluate whether YW3-56 has adverse effects on the growth and the vital organ functions in mouse, we measured the body as well as brain, heart, liver, kidney, and spleen weight after drug treatment. Daily injection of YW3-56 at 10 mg/kg of

body weight for 1 week did not decrease the size of mouse body or organs, suggesting that the adverse effects of YW3-56 are low if any (supplemental Fig. S9). Moreover, SAHA alone or YW3-56 and SAHA in combination did not impair mouse growth or sizes of vital organs (supplemental Fig. S9). In contrast, the size of the spleen was decreased to ~50% of that of control mice after doxorubicin treatment (supplemental Fig. S9), suggesting that inhibitors targeting PAD4 and HDACs are less toxic when compared with doxorubicin. Additionally, we performed a 3-month YW3-56 treatment experiment with a daily injection of YW3-56 at 10 mg/kg of body weight in a pair of nude mice and determined that the sizes of the mouse body and vital organs were not altered after YW3-56 treatment.

## DISCUSSION

An emerging theme in the field of cancer research is that the epigenetic silencing of tumor suppressor genes can lead to increased cell growth and cell division during tumorigenesis. Because epigenetic alterations do not include mutations in DNA *per se*, tumor suppressor genes can be turned back on by

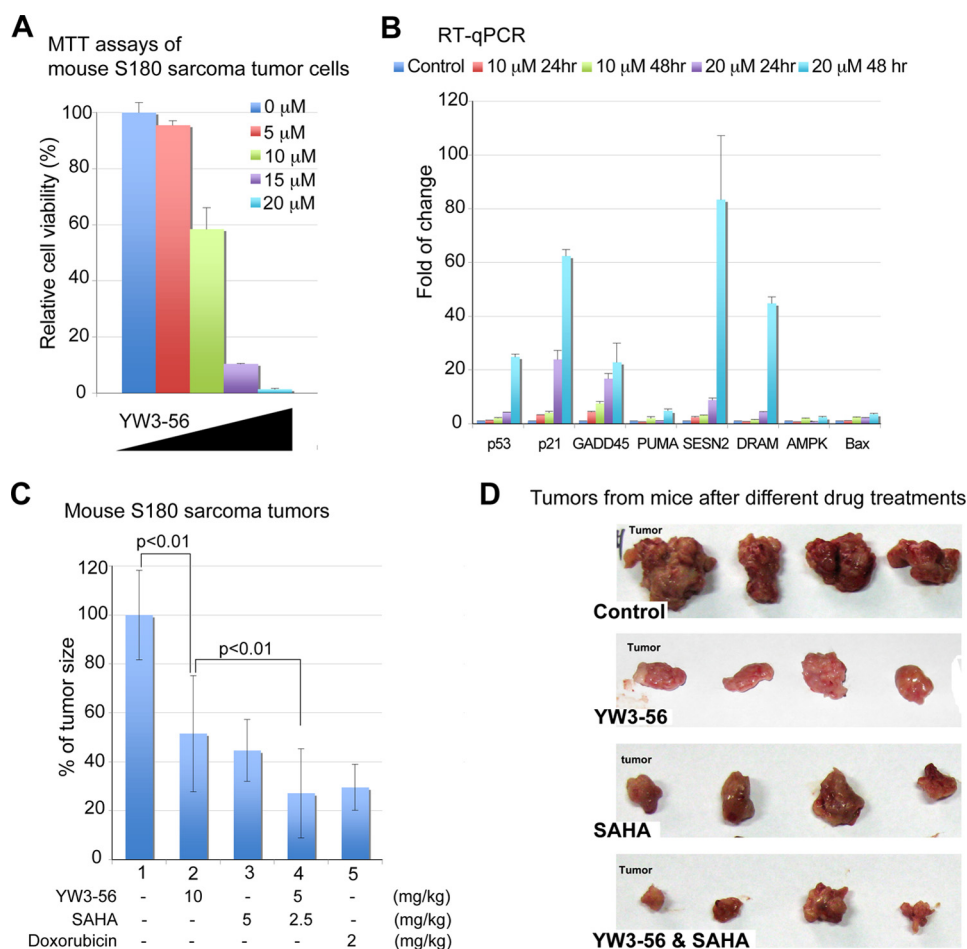


**FIGURE 7. YW3-56 inhibits tumor growth in a mouse tumor model and cooperates with the HDAC inhibitor SAHA.** A, the growth inhibition of mouse sarcoma S-180 cells after YW3-56 treatment was analyzed by MTT assays (averages and standard deviations are shown,  $n = 3$ ). B, p53 and its target gene expression levels were analyzed by RT-qPCR in S-180 cells after YW3-56 treatment (averages and standard deviations are shown,  $n = 3$ ). DRAM, damage-regulated autophagy modulator; AMPK, AMP-activated protein kinase. C, growth inhibition of S-180 cell-derived tumors in mice by YW3-56, SAHA, a combination of YW3-56 and SAHA, or doxorubicin. In total, 27 mice for control, 21 mice for YW3-56, 11 mice for SAHA, 11 mice for SAHA and YW3-56, and 15 mice for doxorubicin treatment from the above two independent experiments were used to collect data for tumor sizes and body/organ weights. Averages and standard deviations are shown. Statistical analyses were performed using Student's  $t$  test. D, representative images showing the tumor mass in control mice and mice after YW3-56, SAHA, or a combination of YW3-56 and SAHA treatment.

targeting epigenetic modifiers, as evidenced by recent progression in this area (3–5). Previous pathological and genetic studies have linked PAD4 and protein Arg citrullination with several human diseases, including cancers and autoimmune disorders. In cancer cells, a fine-tuned increase of PAD4 protein represses the expression of p53 target genes, such as p21/*CDKN1A*, *GADD45*, and *PUMA*. Here, using the newly developed PAD inhibitors, we identified a novel molecular mechanism by which PAD4 represses the expression of the p53 target gene *SESN2* to promote cancer cell growth, suggesting that PAD4 may facilitate tumorigenesis from multiple aspects. The lead compound YW3-56 demonstrates tumor growth inhibition effects singularly or in combination with SAHA, whereas it has little if any detectable side effects under the conditions applied. Given that PAD4 is overexpressed in the majority of human cancers of many tissue origins and that its levels are elevated in the blood of cancer patients (21), further investigation of PAD4 and its inhibitors is of important value in cancer diagnosis and treatment.

Cancer cells respond very fast to YW3-56 treatment. As quick as 6 h after YW3-56 addition to U2OS cells, we observed

changes in cell morphology, such as a loss of cell attachment and formation of cytosolic bubbles. This fast kinetics is in agreement with the high membrane permeability and accumulation in cancer cells detected by flow cytometry analyses as well as the immediate induction of the *SESN2* and *DDIT4* gene expression within hours after the drug treatment. Autophagy represents an important cellular adaptation response to various stress signals (37, 38, 52). Starvation leads to the activation of several signaling pathways including the p53-*SESN2* axis. Once expressed, *SESN2* can work together with the TSC1-TSC2 protein complex to inhibit the mTORC1 complex-mediated phosphorylation of its target proteins that are involved in protein synthesis. The decreased rate of protein translation is coupled with a concomitant increase of cellular autophagy. Our siRNA results showed that *SESN2* is directly regulated by PAD4 and is a sufficient factor for regulating the phosphorylation of mTORC1 substrate p70S6K. YW3-56 activates the expression of *SESN2* and inhibits the phosphorylation of p70S6K, offering a mechanism by which YW3-56 may induce autophagy. Moreover, YW3-56 treatment leads to the accumulation of both autophagosomes and autophagolysosomes as well as the accu-

mulation of p62/SQSTM1, suggesting that it exacerbates the autophagy burden by inhibiting autophagic vesicle degradation. Our ongoing research will further unveil the molecular and cellular mechanisms underlying the YW3-56 activity to curb cancer cell growth.

Cl-amidine was originally designed as a structural mimic of the PAD substrate peptidylarginine by the Thompson group (44). Cl-amidine shows a broad inhibition of all active PAD family members, albeit at different efficiency (PAD1>PAD4>PAD3>PAD2) (45). Our work has found that Cl-amidine exerts 50% tumor growth inhibition at ~150–200  $\mu$ M concentrations (24). In this study, we developed a set of novel PAD inhibitors by an extensive structure-and-activity relationship study based on the chloroacetamide functional group, which covalently modifies the active center cysteine of the PAD enzymes (44). The lead compound YW3-56 inhibits cancer cell growth at low micromolar concentrations, showing >60-fold increase in cancer growth inhibition over Cl-amidine. This gain in YW3-56 inhibitor efficacy is due to two possible factors: 1) a mild increase in PAD4 inhibition achieved by optimizing the backbone; and 2) a large increase in the membrane permeability of YW3-56 by the addition of a more hydrophobic dimethyl-amide-naphthalene moiety at the  $N\alpha$  position and a phenyl ring at the  $C\alpha$  position. In parallel to our study, the Thompson group (45, 55) has recently reported two additional structures related to Cl-amidine by adding one or two amino acids to the  $N\alpha$  position of Cl-amidine. Given that these inhibitors are all developed on a mechanism-based design, they need to compete with the *in vivo* PAD substrates to achieve efficient inhibition. Allosteric effect inhibition may represent a future strategy to develop additional inhibitors. On the other hand, the current experimental data found that mechanism-based PAD inhibitors derived from the Cl-amidine backbone show pharmacological efficacy both in cell culture and in mouse models, suggesting that this strategy may prove to be viable in future pharmacology exploration.

The PAD family of contains five members in human and mouse, including PAD1–4 and PAD6, that show tissue and substrate specificity (56, 57). A recent study with PAD2, PAD3, and PAD4 enzymes found that PAD4 prefers histone H3, whereas PAD2 prefers actin for citrullination (11). However, the interaction of PAD4 with its substrate peptides is mainly mediated by the peptide backbone (58), suggesting that PAD4 may target Arg residues embedded in a diverse range of substrates. To date, histones H3, H4, and H2A, ING4, nucleophosmin, and nuclear lamin C have been identified as substrate of PAD4. This imposes a future challenge in addressing the function of PAD4 in targeting these particular substrates. On the other hand, the loose substrate context dependence of PAD proteins likely imposes additional challenges to developing isoform-specific PAD inhibitors for biology and preclinical studies. The lead compound YW3-56 can inhibit both PAD2 and PAD4. At the current stage of our inhibitor and drug development, the broad inhibition of YW3-56 to PAD enzymes should not be a concern for clinical application given that many effective cancer therapies target general cellular processes and successful epigenetic inhibitors used in cancer therapy often target

a family of enzymes, such as the DNA methyltransferase inhibitors and the histone deacetylase inhibitors.

**Acknowledgments**—We thank members of the Chen and Wang groups as well as the Center for Eukaryotic Gene Regulation for helpful discussions and comments and Sarah L. Moore for editing the manuscript. We thank Drs. Siqi Peng and Ming Zhao at Capital Medical University, Beijing, China for support and comments on the work. The mCherry-GFP-LC3 is a generous gift from Dr. Terje Johansen. We thank Dr. Tso-Pang Yao for reagents. We thank the Penn State University (PSU) Microscopy and Cytometry Facility and the Genomics Core Facility for technical help. A patent application based on this work was submitted.

**Addendum**—In the first paragraph under “Experimental Procedures” of the online published manuscript, we cited Ref. 44 (Luo *et al.*, *Biochemistry*, 2006), the original paper that developed the synthesis method of Cl-amidine by Dr. Thompson’s group. However, because we used a solution-based synthesis scheme to generate PAD inhibitors in our study, the paper published by the Thompson group (Causey and Thompson, *Tetrahedron Letters*, 2008) describing the solution phase synthesis of Cl-amidine should be a more appropriate reference (59) to be cited in addition to Ref. 44.

## REFERENCES

- Li, B., Carey, M., and Workman, J. L. (2007) The role of chromatin during transcription. *Cell* **128**, 707–719
- Conaway, J. W. (2012) Introduction to theme “chromatin, epigenetics, and transcription.” *Annu. Rev. Biochem.* **81**, 61–64
- Chi, P., Allis, C. D., and Wang, G. G. (2010) Covalent histone modifications: miswritten, misinterpreted, and mis-erased in human cancers. *Nat. Rev. Cancer* **10**, 457–469
- Sandoval, J., and Esteller, M. (2012) Cancer epigenomics: beyond genomics. *Curr. Opin. Genet. Dev.* **22**, 50–55
- Wang, G. G., and Allis, C. D. (2009) “Misinterpretation” of a histone mark is linked to aberrant stem cells and cancer development. *Cell Cycle* **8**, 1982–1983
- Yoo, C. B., and Jones, P. A. (2006) Epigenetic therapy of cancer: past, present, and future. *Nat. Rev. Drug Discov.* **5**, 37–50
- Daigle, S. R., Olhava, E. J., Therkelsen, C. A., Majer, C. R., Sneeringer, C. J., Song, J., Johnston, L. D., Scott, M. P., Smith, J. J., Xiao, Y., Jin, L., Kuntz, K. W., Chesworth, R., Moyer, M. P., Bernt, K. M., Tseng, J. C., Kung, A. L., Armstrong, S. A., Copeland, R. A., Richon, V. M., and Pollock, R. M. (2011) Selective killing of mixed lineage leukemia cells by a potent small-molecule DOT1L inhibitor. *Cancer Cell* **20**, 53–65
- Delmore, J. E., Issa, G. C., Lemieux, M. E., Rahl, P. B., Shi, J., Jacobs, H. M., Kasttrit, E., Gilpatrick, T., Paranal, R. M., Qi, J., Chesi, M., Schinzel, A. C., McKeown, M. R., Heffernan, T. P., Vakoc, C. R., Bergsagel, P. L., Ghobrial, I. M., Richardson, P. G., Young, R. A., Hahn, W. C., Anderson, K. C., Kung, A. L., Bradner, J. E., and Mitsiades, C. S. (2011) BET bromodomain inhibition as a therapeutic strategy to target c-Myc. *Cell* **146**, 904–917
- Zuber, J., Shi, J., Wang, E., Rappaport, A. R., Herrmann, H., Sison, E. A., Magoon, D., Qi, J., Blatt, K., Wunderlich, M., Taylor, M. J., Johns, C., Chicas, A., Mulloy, J. C., Kogan, S. C., Brown, P., Valent, P., Bradner, J. E., Lowe, S. W., and Vakoc, C. R. (2011) RNAi screen identifies Brd4 as a therapeutic target in acute myeloid leukemia. *Nature* **478**, 524–528
- Vossenaar, E. R., Zendman, A. J., van Venrooij, W. J., and Pruijn, G. J. (2003) PAD, a growing family of citrullinating enzymes: genes, features, and involvement in disease. *Bioessays* **25**, 1106–1118
- Darrah, E., Rosen, A., Giles, J. T., and Andrade, F. (2012) Peptidylarginine deiminase 2, 3, and 4 have distinct specificities against cellular substrates: novel insights into autoantigen selection in rheumatoid arthritis. *Ann. Rheum. Dis.* **71**, 92–98
- Wright, P. W., Bolling, L. C., Calvert, M. E., Sarmiento, O. F., Berkeley, E. V., Shea, M. C., Hao, Z., Jayes, F. C., Bush, L. A., Shetty, J., Shore, A. N.,

- Reddi, P. P., Tung, K. S., Samy, E., Allietta, M. M., Sherman, N. E., Herr, J. C., and Coonrod, S. A. (2003) ePAD, an oocyte and early embryo-abundant peptidylarginine deiminase-like protein that localizes to egg cytoplasmic sheets. *Dev. Biol.* **256**, 73–88
13. Kan, R., Yurttas, P., Kim, B., Jin, M., Wo, L., Lee, B., Gosden, R., and Coonrod, S. A. (2011) Regulation of mouse oocyte microtubule and organelle dynamics by PADI6 and the cytoplasmic lattices. *Dev. Biol.* **350**, 311–322
14. Zhang, X., Gamble, M. J., Stadler, S., Cherrington, B. D., Causey, C. P., Thompson, P. R., Roberson, M. S., Kraus, W. L., and Coonrod, S. A. (2011) Genome-wide analysis reveals PADI4 cooperates with Elk-1 to activate c-Fos expression in breast cancer cells. *PLoS Genet.* **7**, e1002112
15. Nakashima, K., Hagiwara, T., Ishigami, A., Nagata, S., Asaga, H., Kuramoto, M., Senshu, T., and Yamada, M. (1999) Molecular characterization of peptidylarginine deiminase in HL-60 cells induced by retinoic acid and 1 $\alpha$ ,25-dihydroxyvitamin D<sub>3</sub>. *J. Biol. Chem.* **274**, 27786–27792
16. Wang, Y., Wysocka, J., Sayegh, J., Lee, Y. H., Perlin, J. R., Leonelli, L., Sonbuchner, L. S., McDonald, C. H., Cook, R. G., Dou, Y., Roeder, R. G., Clarke, S., Stallcup, M. R., Allis, C. D., and Coonrod, S. A. (2004) Human PAD4 regulates histone arginine methylation levels via demethylation. *Science* **306**, 279–283
17. Lee, Y. H., Coonrod, S. A., Kraus, W. L., Jelinek, M. A., and Stallcup, M. R. (2005) Regulation of coactivator complex assembly and function by protein arginine methylation and demethylation. *Proc. Natl. Acad. Sci. U.S.A.* **102**, 3611–3616
18. Guo, Q., and Fast, W. (2011) Citrullination of inhibitor of growth 4 (ING4) by peptidylarginine deiminase 4 (PAD4) disrupts the interaction between ING4 and p53. *J. Biol. Chem.* **286**, 17069–17078
19. Tanikawa, C., Espinosa, M., Suzuki, A., Masuda, K., Yamamoto, K., Tsuchiya, E., Ueda, K., Daigo, Y., Nakamura, Y., and Matsuda, K. (2012) Regulation of histone modification and chromatin structure by the p53-PADI4 pathway. *Nat. Commun.* **3**, 676
20. Suzuki, A., Yamada, R., Chang, X., Tokuhira, S., Sawada, T., Suzuki, M., Nagasaki, M., Nakayama-Hamada, M., Kawaida, R., Ono, M., Ohtsuki, M., Furukawa, H., Yoshino, S., Yukioka, M., Tohma, S., Matsubara, T., Wakitan, S., Teshima, R., Nishioka, Y., Sekine, A., Iida, A., Takahashi, A., Tsunoda, T., Nakamura, Y., and Yamamoto, K. (2003) Functional haplotypes of PADI4, encoding citrullinating enzyme peptidylarginine deiminase 4, are associated with rheumatoid arthritis. *Nat. Genet.* **34**, 395–402
21. Chang, X., Han, J., Pang, L., Zhao, Y., Yang, Y., and Shen, Z. (2009) Increased PADI4 expression in blood and tissues of patients with malignant tumors. *BMC Cancer* **9**, 40
22. Wang, L., Chang, X., Yuan, G., Zhao, Y., and Wang, P. (2010) Expression of peptidylarginine deiminase type 4 in ovarian tumors. *Int. J. Biol. Sci.* **6**, 454–464
23. Chang, X., Hou, X., Pan, J., Fang, K., Wang, L., and Han, J. (2011) Investigating the pathogenic role of PADI4 in esophageal cancer. *Int. J. Biol. Sci.* **7**, 769–781
24. Li, P., Yao, H., Zhang, Z., Li, M., Luo, Y., Thompson, P. R., Gilmour, D. S., and Wang, Y. (2008) Regulation of p53 target gene expression by peptidylarginine deiminase 4. *Mol. Cell Biol.* **28**, 4745–4758
25. Li, P., Wang, D., Yao, H., Doret, P., Hao, G., Shen, Q., Qiu, H., Zhang, X., Wang, Y., and Chen, G. (2010) Coordination of PAD4 and HDAC2 in the regulation of p53 target gene expression. *Oncogene* **29**, 3153–3162
26. Kruse, J. P., and Gu, W. (2009) Modes of p53 regulation. *Cell* **137**, 609–622
27. Crichton, D., Wilkinson, S., O'Prey, J., Syed, N., Smith, P., Harrison, P. R., Gasco, M., Garrone, O., Crook, T., and Ryan, K. M. (2006) DRAM, a p53-induced modulator of autophagy, is critical for apoptosis. *Cell* **126**, 121–134
28. Tang, Y., Luo, J., Zhang, W., and Gu, W. (2006) Tip60-dependent acetylation of p53 modulates the decision between cell cycle arrest and apoptosis. *Mol. Cell* **24**, 827–839
29. Li, X., Wu, L., Corsa, C. A., Kunkel, S., and Dou, Y. (2009) Two mammalian MOF complexes regulate transcription activation by distinct mechanisms. *Mol. Cell* **36**, 290–301
30. Vousden, K. H., and Prives, C. (2009) Blinded by the light: the growing complexity of p53. *Cell* **137**, 413–431
31. Wei, C. L., Wu, Q., Vega, V. B., Chiu, K. P., Ng, P., Zhang, T., Shahab, A., Yong, H. C., Fu, Y., Weng, Z., Liu, J., Zhao, X. D., Chew, J. L., Lee, Y. L., Kuznetsov, V. A., Sung, W. K., Miller, L. D., Lim, B., Liu, E. T., Yu, Q., Ng, H. H., and Ruan, Y. (2006) A global map of p53 transcription factor binding sites in the human genome. *Cell* **124**, 207–219
32. Harris, S. L., and Levine, A. J. (2005) The p53 pathway: positive and negative feedback loops. *Oncogene* **24**, 2899–2908
33. Budanov, A. V., and Karin, M. (2008) p53 target genes sestrin1 and sestrin2 connect genotoxic stress and mTOR signaling. *Cell* **134**, 451–460
34. Maiuri, M. C., Malik, S. A., Morselli, E., Kepp, O., Criollo, A., Mouchel, P. L., Carnuccio, R., and Kroemer, G. (2009) Stimulation of autophagy by the p53 target gene Sestrin2. *Cell Cycle* **8**, 1571–1576
35. Tanikawa, C., Ueda, K., Nakagawa, H., Yoshida, N., Nakamura, Y., and Matsuda, K. (2009) Regulation of protein Citrullination through p53/PADI4 network in DNA damage response. *Cancer Res.* **69**, 8761–8769
36. Mizushima, N., Levine, B., Cuervo, A. M., and Klionsky, D. J. (2008) Autophagy fights disease through cellular self-digestion. *Nature* **451**, 1069–1075
37. Kroemer, G., Mariño, G., and Levine, B. (2010) Autophagy and the integrated stress response. *Mol. Cell* **40**, 280–293
38. Yang, Z., and Klionsky, D. J. (2010) Mammalian autophagy: core molecular machinery and signaling regulation. *Curr. Opin. Cell Biol.* **22**, 124–131
39. Mathew, R., Karantza-Wadsworth, V., and White, E. (2007) Role of autophagy in cancer. *Nat. Rev. Cancer* **7**, 961–967
40. Dunlop, E. A., and Tee, A. R. (2009) Mammalian target of rapamycin complex 1: signaling inputs, substrates, and feedback mechanisms. *Cell. Signal.* **21**, 827–835
41. Amaravadi, R. K., Lippincott-Schwartz, J., Yin, X. M., Weiss, W. A., Takebe, N., Timmer, W., DiPaola, R. S., Lotze, M. T., and White, E. (2011) Principles and current strategies for targeting autophagy for cancer treatment. *Clin. Cancer Res.* **17**, 654–666
42. Berardi, D. E., Campodónico, P. B., Díaz Bessone, M. I., Urtreger, A. J., and Todaro, L. B. (2011) Autophagy: friend or foe in breast cancer development, progression, and treatment. *Int. J. Breast Cancer* **2011**, 595092
43. Li, P., Li, M., Lindberg, M. R., Kennett, M. J., Xiong, N., and Wang, Y. (2010) PAD4 is essential for antibacterial innate immunity mediated by neutrophil extracellular traps. *J. Exp. Med.* **207**, 1853–1862
44. Luo, Y., Arita, K., Bhatia, M., Knuckley, B., Lee, Y. H., Stallcup, M. R., Sato, M., and Thompson, P. R. (2006) Inhibitors and inactivators of protein arginine deiminase 4: functional and structural characterization. *Biochemistry* **45**, 11727–11736
45. Jones, J. E., Slack, J. L., Fang, P., Zhang, X., Subramanian, V., Causey, C. P., Coonrod, S. A., Guo, M., and Thompson, P. R. (2012) Synthesis and screening of a haloacetamide containing library to identify PAD4 selective inhibitors. *ACS Chem. Biol.* **7**, 160–165
46. Wang, W., Zhao, M., Wang, Y., Liu, J., Wu, J., Kang, G., and Peng, S. (2011) {2-[1-(3-Methoxycarbonylmethyl-1H-indol-2-yl)-1-methyl-ethyl]-1H-indol-3-yl}-acetic acid methyl ester (MIAM): its anticancer efficacy and intercalation mechanism identified via multimodel systems. *Mol. Biosyst.* **7**, 766–772
47. Boyde, T. R., and Rahmatullah, M. (1980) Optimization of conditions for the colorimetric determination of citrulline, using diacetyl monoxime. *Anal. Biochem.* **107**, 424–431
48. Hao, G., Wang, D., Gu, J., Shen, Q., Gross, S. S., and Wang, Y. (2009) Neutral loss of isocyanic acid in peptide CID spectra: a novel diagnostic marker for mass spectrometric identification of protein citrullination. *J. Am. Soc. Mass Spectrom.* **20**, 723–727
49. Ellisen, L. W., Ramsayer, K. D., Johannessen, C. M., Yang, A., Beppu, H., Minda, K., Oliner, J. D., McKeon, F., and Haber, D. A. (2002) REDD1, a developmentally regulated transcriptional target of p63 and p53, links p63 to regulation of reactive oxygen species. *Mol. Cell* **10**, 995–1005
50. Nakashima, K., Hagiwara, T., and Yamada, M. (2002) Nuclear localization of peptidylarginine deiminase V and histone deimination in granulocytes. *J. Biol. Chem.* **277**, 49562–49568
51. Hara, K., Yonezawa, K., Kozlowski, M. T., Sugimoto, T., Andrabi, K., Weng, Q. P., Kasuga, M., Nishimoto, I., and Avruch, J. (1997) Regulation of eIF-4E BP1 phosphorylation by mTOR. *J. Biol. Chem.* **272**, 26457–26463
52. Mizushima, N., Yoshimori, T., and Levine, B. (2010) Methods in mamma-

- lian autophagy research. *Cell* **140**, 313–326
53. Bjørkøy, G., Lamark, T., Brech, A., Outzen, H., Perander, M., Overvatn, A., Stenmark, H., and Johansen, T. (2005) p62/SQSTM1 forms protein aggregates degraded by autophagy and has a protective effect on huntingtin-induced cell death. *J. Cell Biol.* **171**, 603–614
  54. Alfaro, G., Lomeli, C., Ocadiz, R., Ortega, V., Barrera, R., Ramirez, M., and Nava, G. (1992) Immunologic and genetic characterization of S180, a cell line of murine origin capable of growing in different inbred strains of mice. *Vet Immunol. Immunopathol.* **30**, 385–398
  55. Causey, C. P., Jones, J. E., Slack, J. L., Kamei, D., Jones, L. E., Subramanian, V., Knuckley, B., Ebrahimi, P., Chumanevich, A. A., Luo, Y., Hashimoto, H., Sato, M., Hofseth, L. J., and Thompson, P. R. (2011) The development of *N*- $\alpha$ -(2-carboxyl)benzoyl-*N*<sup>5</sup>-(2-fluoro-1-iminoethyl)-l-ornithine amide (*o*-F-amidine) and *N*- $\alpha$ -(2-carboxyl)benzoyl-*N*<sup>5</sup>-(2-chloro-1-iminoethyl)-l-ornithine amide (*o*-Cl-amidine) as second generation protein arginine deiminase (PAD) inhibitors. *J. Med. Chem.* **54**, 6919–6935
  56. Vossenaar, E. R., Radstake, T. R., van der Heijden, A., van Mansum, M. A., Dieteren, C., de Rooij, D. J., Barrera, P., Zendman, A. J., and van Venrooij, W. J. (2004) Expression and activity of citrullinating peptidylarginine deiminase enzymes in monocytes and macrophages. *Ann. Rheum. Dis.* **63**, 373–381
  57. Ying, S., Dong, S., Kawada, A., Kojima, T., Chavanas, S., Méchin, M. C., Adoue, V., Serre, G., Simon, M., and Takahara, H. (2009) Transcriptional regulation of peptidylarginine deiminase expression in human keratinocytes. *J. Dermatol. Sci.* **53**, 2–9
  58. Arita, K., Shimizu, T., Hashimoto, H., Hidaka, Y., Yamada, M., and Sato, M. (2006) Structural basis for histone N-terminal recognition by human peptidylarginine deiminase 4. *Proc. Natl. Acad. Sci. U.S.A.* **103**, 5291–5296
  59. Causey, C. P., and Thompson, P. R. (2008) An improved synthesis of haloacetamidine-based inactivators of protein arginine deiminase 4 (PAD4). *Tetrahedron Lett.* **49**, 4383–4385

**Anticancer Peptidylarginine Deiminase (PAD) Inhibitors Regulate the Autophagy Flux and the Mammalian Target of Rapamycin Complex 1 Activity**

Yuji Wang, Pingxin Li, Shu Wang, Jing Hu, Xiangyun Amy Chen, Jianhui Wu, Megan Fisher, Kira Oshaben, Na Zhao, Ying Gu, Dong Wang, Gong Chen and Yanming Wang

*J. Biol. Chem.* 2012, 287:25941-25953.

doi: 10.1074/jbc.M112.375725 originally published online May 17, 2012

---

Access the most updated version of this article at doi: [10.1074/jbc.M112.375725](https://doi.org/10.1074/jbc.M112.375725)

Alerts:

- [When this article is cited](#)
- [When a correction for this article is posted](#)

[Click here](#) to choose from all of JBC's e-mail alerts

Supplemental material:

<http://www.jbc.org/content/suppl/2012/05/17/M112.375725.DC1>

This article cites 59 references, 14 of which can be accessed free at <http://www.jbc.org/content/287/31/25941.full.html#ref-list-1>